HIGH SENSITIVITY PHOSPHATE ION SENSOR BASED ON GRAPHENE OXIDE FIELD-EFFECT TRANSISTOR

by

Bing Jin

A Thesis Submitted in

Partial Fulfillment of the

Requirements for the Degree of

Master of Science

in Engineering

at

The University of Wisconsin-Milwaukee

May 2018

ABSTRACT

HIGH SENTIVITY PHOSPHATE ION SENSOR BASED ON GRAPHENE OXIDE FIELD-EFFECT TRANSISTOR

by

Bing Jin

The University of Wisconsin-Milwaukee, 2018
Under the Supervision of Professor Junhong Chen

Excessive phosphates in water can lead to eutrophication and algae growth. Management of phosphorus in water requires accurate and accessible detection technologies to ensure real-time monitoring of phosphorus. Current sensing technologies for phosphorus have limitations and disadvantages. This thesis study will explore a low-cost, ultrasensitive, and real-time water sensor for monitoring phosphates in agriculture runoff, wastewater, and surface water by collaborating with MWRD (Metropolitan Water Reclamation District of Greater Chicago), Grande Cheese Company and Wisconsin DNR (Department of Natural Resources). The innovative sensing technology takes advantage of nanomaterial advancements to realize real-time phosphorus detection.

Specifically, we report an ultrasensitive phosphate ion sensor based on field-effect transistor with reduced graphene oxide (rGO) as the channel material (GOFET). To avoid interference response, a thin aluminum oxide layer (Al_2O_3, ~4 nm thickness) was applied in our work to isolate graphene oxide sheet (GO) from detection solution samples, and gold nanoparticles (AuNP ~2 nm diameter) were deposited on the Al_2O_3 film surface for ferritin probe modification. After annealing under argon environment, rGO demonstrated a good current on/off ratio and p-type semiconductor FET performance. The sensing test results showed that the sensor responded

to phosphate ions instantaneously and ferritin probes had good affinity to phosphate ions in water solutions. The lower limit of detection for the sensor can reach down to 0.025 mg/L in real water samples.

The low-cost microsensor can provide a new opportunity for real-time monitoring of phosphates. The project results will benefit water industry, agriculture, and environmental regulators by providing real-time sensing capabilities for phosphorus aiming for better evaluation and control of water quality or improving the operation efficiency of phosphate removal in wastewater treatment.

TABLE OF CONTENTS

LIST OF FIGURES

LIST OF TABLES

LIST OF ABBREVIATIONS

GO	Graphene oxide
FET	Field-Effect Transistor
rGO	Reduced graphene oxide
SEM	Scanning electron microscopy
AET	Cysteamine
GA	Glutaraldehyde
AuNPs	Gold nanoparticles
ALD	Atomic Layer Deposition
PDMS	Polydimethylsiloxane
s-GQDs-Al^{3+}	Single-layered graphene quantum dots – Al^{3+}
HEMTs	High electron mobility transistors
Cu(II)Pc-PAA	Copper Phthalocyanine – Acrylate - polymer

ACKNOWLEDGEMENTS

Foremost, I would like to express my sincere gratitude to my advisor Prof. Junhong Chen for the continuous support of my Master's study, for his patience, motivation, enthusiasm, and immense knowledge. His guidance helped me throughout my research and writing of this thesis. I could not have imagined having a better advisor and mentor for my Master's study.

Besides my advisor, I would like to thank the rest of my thesis committee, Prof. Deyang Qu and Prof. Yin Wang, for their encouragement, insightful comments, and hard questions.
I thank my fellow labmates in the Nanotechnology for Sustainable Energy and Environment Laboratory: Haihui Pu, Arnab Maity and Jingbo Chang, for the stimulating discussions, for the unconditional teaching of water sensor working principles. Also, I thank Qianqian Dong and Xiaoyu Sui for research support and very helpful suggestions, and for the fun we had in the last two years. I would also like to thank all the other members of my research group for their help.

Last but not least, I would like to thank my family: my wife Mian Liu, my mother-in-law Xiaoyan Xu, and my parents, for always standing by me, understanding me and supporting me.

CHAPTER 1 INTRODUCTION AND LITERATURE REVIEW

1.1 Background

Graphene oxide as one of carbon nanomaterials in graphene family has been widely investigated for gas sensors [1], biosensors [2], and ion sensors[3]. Although electrical properties of reduced graphene oxide (rGO) are not comparable to those of pristine graphene due to the structural defects [4], there are still many advantages in real applications. In general, it has similar layered structure to graphite, but the carbon sheet is abundantly decorated by oxygen-contained groups, which provide chemical modification sites and make the atomic-thick layers hydrophilic. Additionally, on the nanoscale, because of thin graphene-based sheets, this carbon-based material exhibits a high specific surface area. The most attractive and potential property of GO is that it can be reduced to graphene-like sheets by removing the oxygen-contained groups, e.g., under 400 °C in flowing Argon environment [5]. After annealing, the fully reduced monolayer reduced graphene oxide (rGO) exhibited conductivities ranging between 0.05 and 2 S/cm and field effect mobilities of 2-200 cm^2/Vs at room temperature [6].

On the other hand, regarding the nanoelectronics, rGO or graphene, provides a versatile platform for a wide spectrum of sensing applications based on various mechanisms including: charge transfer, charge scattering, capacitive effect, and field effect. The field effect has been regarded as the most reliable sensing mechanism which can be modulated by the electrical conductivity of a material upon the application of an external electric field, for instance, induced by the adsorbed charged biomolecules. Until now, these nanoscale carbon materials including graphene, reduced graphene oxide have been widely reported in application combined with field-effect transistor (FET) for detecting ions [7], proteins [8], DNA [9], cells [10]. In Shun's work [11], they

reported a reduced graphene oxide-based FET platform for orthophosphate ion detection, from which achieved a limit of detection down to 0.806 ug/L and a response time on the order of seconds.

Phosphorus is one of the key elements necessary for the growth of plants and animals in water ecosystems. In instances where phosphorus is a growth-limiting nutrient, the discharge of raw or treated wastewater, agricultural drainage, or certain industrial wastes may stimulate the growth of photosynthetic aquatic micro- and macroorganisms in large quantities. Phosphates enter waterways from human and animal waste, phosphorus rich bedrock, laundry, cleaning, industrial effluents, and agriculture runoff, which become harmful when they over fertilize aquatic plants and cause eutrophication.

In this work, we will introduce a stable sensor platform based the rGO-FET for phosphate ions detection in the real water sample. Many literatures have introduced that graphene has excellent adsorption properties due to its unique carbon sheet structure [12-14]. To avoid this interference, we used aluminum oxide film coating on the rGO surface to separate the rGO from the sample solution. There exist two main mechanisms to affect the FET performance: charge transfer and gate effect. This aluminum oxide film will also block the charge transfer between rGO and phosphate ions. To support modification sites for ferritin probes, we deposited 2 nm thickness gold nanoparticles on aluminum oxide surface. Based on this designed sensor platform for phosphate detection, the performance is more reliable, and limit of detection can be down to 0.025 mg/L.

1.2 Introduction

As one of the most attractive nanomaterials in the past decade, graphene sensors have been researched and reported due to its unique properties, including mechanical, electrical applications. The sensing principle based on a change of the electrical conductance of the graphene channel

upon adsorption of a molecule on the sensor surface. The uniqueness of graphene among other solid-state materials is that all carbon atoms are located on the surface, making the graphene surface potentially highly sensitive to any changes of its surrounding environment. Thank of the excellent electrical properties of graphene, such as extraordinary high mobility (15, 000 $cm^2V^{-1}s^{-1}$)[6] and low intrinsic electrical noise[15], graphene-FET (GFET) electronic sensors displaced greater sensitivity than traditional assays. Besides, graphene has a crystal lattice free of dangling bonds and is therefore intrinsically chemically inert. This inertness has been a driving force for the first attempts aiming at bio interfacing graphene with specific recognition moieties, vis both covalent[16] and non-covalent[17] approaches, using different biochemical molecules and chemical treatments, as shown in Table 1. Evaluation about the electronic, i.e., the high carrier mobility, low intrinsic electrical noise and the inert chemical properties, which are at the core of the sensing mechanisms but also crucial in applications where graphene must be interfaced with biological systems[18].

Table 1. Sensing performances of GFETs for selected analytes.

Analyte	Probe	Limit of detection	Ref.
NO_2 gas	**PNS**	**20 p.p.b.**	[1]
NH_3 gas	**Ag NPs**	**-**	[19]
Hg^+	**TGA**	**25 nM**	[20]
Pb^{2+}	**L-glutathione**	**10 nM**	[5]
E. coli	**Anti-E. coli**	**10 cfu/mL**	[21]
Ebola	**Anti-Ebola**	**1 ng/mL**	[2]

1.2.1 The need for phosphate ion sensors

Phosphorus is one of the basic elements necessary for the growth of plants and animals, especially in lake ecosystems it is important to be the growth-limiting nutrient. Phosphorus mainly exits in nature by phosphates PO_4^{3-} which in three forms: orthophosphate, metaphosphate (or polyphosphate) and organically bound phosphate. Each compound contains phosphorous in a different chemical arrangement [1, 2], as shown in Figure 1. Phosphates are not toxic to people or animals unless they are accumulated in very high level. For example, digestive problems could occur from extremely high levels of phosphate [22]. Additionally, phosphate will stimulate the growth of plankton and aquatic plants which provide food for larger organisms, such as fish, zooplankton and other mammals. However, as the result of enrichment of phosphate, the aging process of lake or surface water ecosystem will be accelerated. This overproduction will lead to an imbalance in the nutrient and material cycling process. Management of phosphorus is a bit of a paradox because, while the world may face a shortage of phosphorus-containing fertilizer later this century, many regions are currently afflicted with an oversupply in both inland and coastal waters causing algal blooms that can produce extremely dangerous toxins that can sicken or kill people or animals, create dead zones in the water, raise treatment costs for drinking water, and hurt industries that depend on clean water. The ability to provide field-deployable, inexpensive, and environmentally-and energetically-sustainable sensors for real-time application and monitoring of phosphorus-containing species while reducing the amount of these species in waste or run-off streams would benefit food production, benefit water quality, and result in significantly less energy consumption.

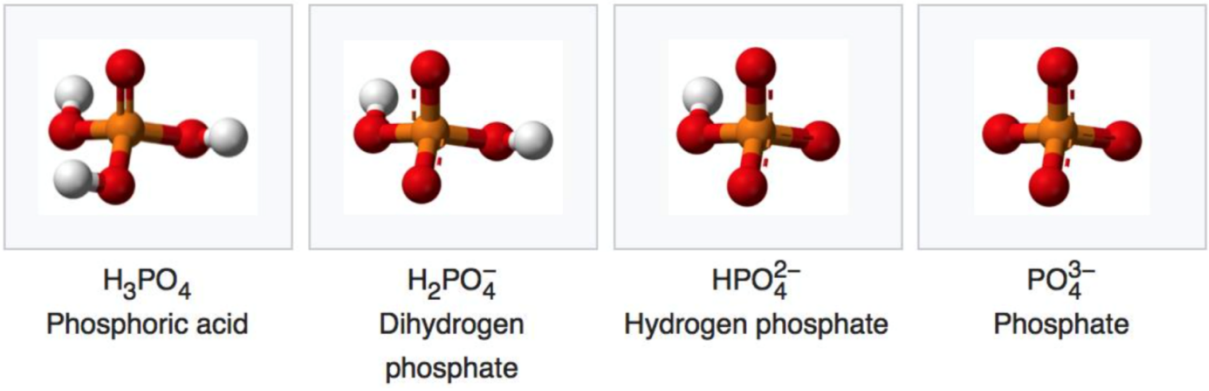

Figure 1. Existing forms of phosphate ions in nature [23].

1.2.2 Graphene oxide properties and applications

As one of members in graphene big family, although electrical properties of reduced graphene oxide (rGO) are not comparable to those of pristine graphene due to structure defects[24], there are still many advantages in real applications. For example, rGO has received great attention as a promising material in a variety of composites such as gas sensor[1], batteries[25], photodetectors[26], or ion detection device[5]. Much effort has been currently devoted to study of the transport properties of graphene, especially focus on as known minimum conductivity problem[27-29]. This interesting topic is so-called charge-neutral point where monolayer graphene's conductivity would drop to a finite minimum value and the density of states should hypothetically vanish (for nondisordered and noninteracting electrons)[27]. Due to the uniqueness of the Fermi level, the electric charge will form conduction band and valence band in the type of positive holes and negative electrons, respectively. At the charge neutral point, graphene is then depicted as a mixture of electrons and holes.

However, in contrast to ultra-clean or pristine graphene, the edges or defections randomly distribute on the graphene oxide surface are chemically reactive and can be relatively easily functionalized, as in Figure 2. Consequently, as the concentration changed of carriers, the charge

neutrality point of Dirac point will strongly demonstrate p/n type shift. From Huang's report [30], n shift of Dirac point would be induced as the ethanol molecules gradually draws electrons from the metal contacts to move to and accumulate on the graphene surface. By contrast, electrons are pushed away from the graphene surface due to the dipole moments of the ethanol molecules are reversed, resulting in a very strong p-type shift of Dirac point. In addition, as the electron/hole in graphene are confined to an atomically thick plane, the electrical conductance, or also as known the carrier concentration, is extremely sensitive to its surroundings such as substrates, dielectric media, and adsorbed foreign molecules[31].

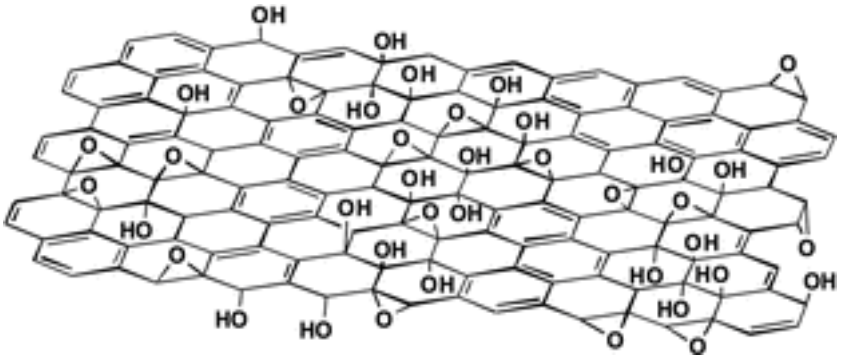

Figure 2. A proposed schematic Lerf-Klinowski of graphene oxide structure [32].

1.3 Literature review

On the phosphate sensor field, lots of semiconductors materials were applied for use at present, as shown in Table 2. Furthermore, sensors in form of potentiometric ion-selective electrodes, amperometric and potential enzyme electrodes, and other devices in the form of integrated probes are also introduced. Optical instrumental now gives very low limit detection, in $nmol^{-1}$ range, but interference from arsenate may be significant. Phosphate biosensor methods can be applied if the number of enzymes participating in the detection scheme is less. Electrochemical sensor platforms showed improved LOD, which are generally rugged, low-cost, and portable.

However, selectivity is hard to be controlled. As a novel ion detection method, FET sensors show a lot of potential in low-concentration and real-time phosphate ion detection. Compared with standard optical enzyme mothed, this electronic sensor could potentially be used for online and real-time monitoring of phosphate ions in surface water. [11]

Table 2. Sensing performance comparison between our sensor and other phosphate sensors

Sensing system	**LOD**	**Linear detection range**	**Calibration slope**	**Ref.**
s-GQDs-Al^{3+}	**100 nM**	**0.25 – 7.5 uM**	**- 0.023**	**33**
AlGaN/GaN HEMTs	**20 nM[1]**	**0.02 – 2 mgL^{-1}**	**3.5 uA/mgL^{-1}**	**34**
Cu(II)Pc-PAA	**1 nM**	**10^{-10} – 10^{-5} M**	**27.7 mV/decade**	**35**
Al-morin/glycidylmethacrylate	**1000 nM**	**0.1 – 1.0 ppm**	**-**	**36**
rGO-FET	**25 nM**	**-**	**-**	**11**

1.3.1 Graphene oxide FET sensor application: the basics for sensing

Detection device based on GFET can be realized through various mechanisms, such as charge transfer, charge scattering, capacitive effect, and field effect. The field effect (modulation of the electrical conductivity of material upon the application of an external electric field, for instance, induced by a charged biomolecule) has been widely introduced as the most reliable

sensing mechanism.[1-3] The typical structure of this GFET as shown in Figure 3 introduces a GFET composed of source/drain metallic electrodes through a graphene channel. The conductivity change of the channel can be typically modulated by the electric field by gating a highly conductive silicon substrate located underneath an insulating SiO_2 dielectric layer to a range of voltages. As shown in Figure 1b, scan in a range of gate voltage and apply a constant bias voltage V_{sd}, between the source and drain, and monitor the resulting current signal I_{sd}. Consequently, the state of charge carriers which flow in the graphene channel can continuously be tuned from holes to electrons, which called "ambipolar behavior". At the minimum current point which is known as the charge neutrality point (CNP).

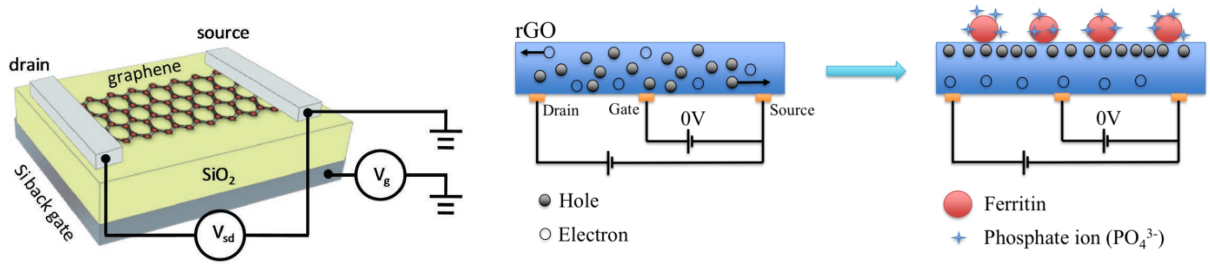

Figure 3. Working principle of a graphene field-effect transistor (GFET) with a back-gated voltage [37].

1.3.2 Challenges of GO-FET sensors

Recently, GFET research trends now to offer new opportunities for developing the next generations label-free biochemical sensors. However, the true potential of graphene sensors in physiological solutions applications is still behind expectations. This is because that GFETs are primarily sensitive to the charges carried by the biomolecules adsorbed on graphene surface, which will suffer from the ionic screening from mobile ions presented in the solution, known as Debye screening effect, shown in Figure 4. Debye screening effect is an intrinsic thermodynamic property

of large systems of mobile charges. In electrolytes, this screening effect is characterized by the Debye length, which is the measure of how far a charge carrier's net electrostatic effect persists, outside of which charges are effectively screened and only 36.8% of the charges can still be seen by the graphene sensing devices [37]. In Shun's work [11], they used rGO-FET for phosphate ions detection, and they quantified this screening effect in terms of the Debye length λ_D of the ion solution,

$$\lambda_D = \frac{1}{\sqrt{4\pi\lambda_B \sum_i C_i Z_i^2}},$$

where λ_B (=0.7 nm at 300k) is the Bjerrum length in water, and $C_i(Z_i)$ is the concentration (valence charge) of ion species i, respectively.

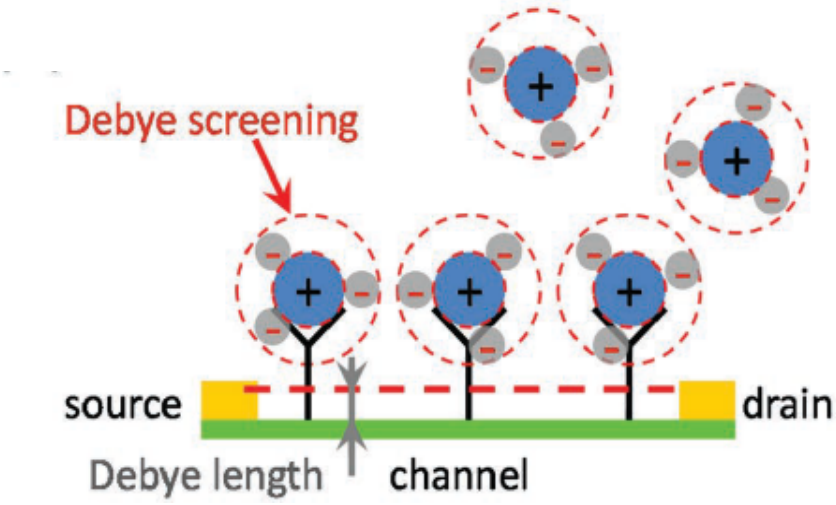

Figure 4. The biomolecules carry zero net charge due to the Debye screening effect of ions in electrolyte [38].

1.4 Organization of thesis

The main research objective of this thesis is to investigate the phosphate sensing characteristics of the graphene oxide FET platform at room temperature and the selectivity of the sensing platform through modifying the sensor surface with ferritin probes.

Chapter 1 presents the background introduction and literature review on the graphene-based FET sensor platform.

Chapter 2 includes all experimental details and structural fabrication of the sensing material and the device.

Chapter 3 presents the electrical properties of GO-FET sensing system.

Chapter 4 focuses on the sensing performance and methods to enhance the sensing performance.

Chapter 5 introduces conclusions and the future work.

CHAPTER 2 FABRICATION AND CHARACTERIZATION OF A PHOSPHATE ION SENSOR

2.1 Fabrication of phosphate ion sensor

This part will introduce the fabrication process details of sensor electrodes. The material of electrode is gold and the total size is 700mm * 800mm. The thickness is 5 nm Ti and 45 nm gold.

2.1.1 Fabrication of GO-FET sensor electrode

In Figure 5, gold interdigital electrodes with a gap of 3 μm were fabricated on a silicon wafer with a top layer of SiO_2 (thickness ~200 nm). from lithography technology uisng a maskless laser writer (MLA-150, Heidelberg InstrumentsCysteamine solution (1 mg/ml) was pipetted onto the sensing area to functionalize the finger electrodes for 30 mins. The functionalized electrode needs to be rinsed with DI water and gently dried by Nitrogen gas. Immersed the cysteamine-assembled electrode in the GO water suspension for 5 seconds. Rinsed by DI water and dried by Nitrogen gas. Then, the GO-modified electrodes were annealed at 400^{o}C under Argon environment for 10 mins to thermally reduce the adhered GO sheets. To passivate this obtained Rgo, a thin Al_2O_3 film will be grown on its surface using atomic layer deposition (ALD, GEMStar XT, Arradiance). Deposited gold nanoparticles on the passivated Rgo surface using a sputter coater for supporting immobilization sites in the next modification steps. Used cysteamine solution again to functionalize the surface of gold NPs for 30 mins, and then added glutaraldehyde solution (5% in water) for another 30 mins. Rinsed in DI water and dried by Nitrogen gas. Ferritin solution (10 mg/l) then pipetted on this assembled area and incubated 3 hours at room temperature.

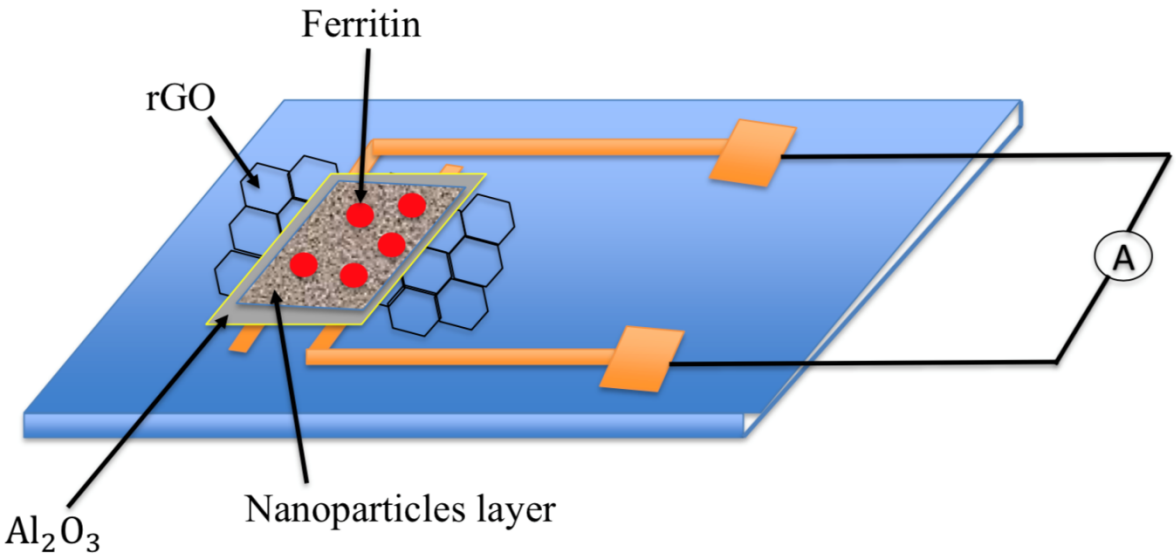

Figure 5. Simplified sensing platform for phosphate ions detection.

2.1.2 Sensing platform modification process

As shown in Figure 6, after depositing ALD and AuNPs on GO surface, 2 ul of 10 ug/ml AET water solution was dropped and incubated about 30 minutes at room temperature. Then washed by DI water and gently dried by air gas. To modify ferritin probe on sensor surface, 2 ul of 5% GA was added and incubated 30 minutes at room temperature. Then washed by DI water and gently dried by air gas. At last, dropped 2 ul of 10 mg/ml ferritin solution and incubated 2 hours at room temperature, then washed by DI water and gently dried by air gas.

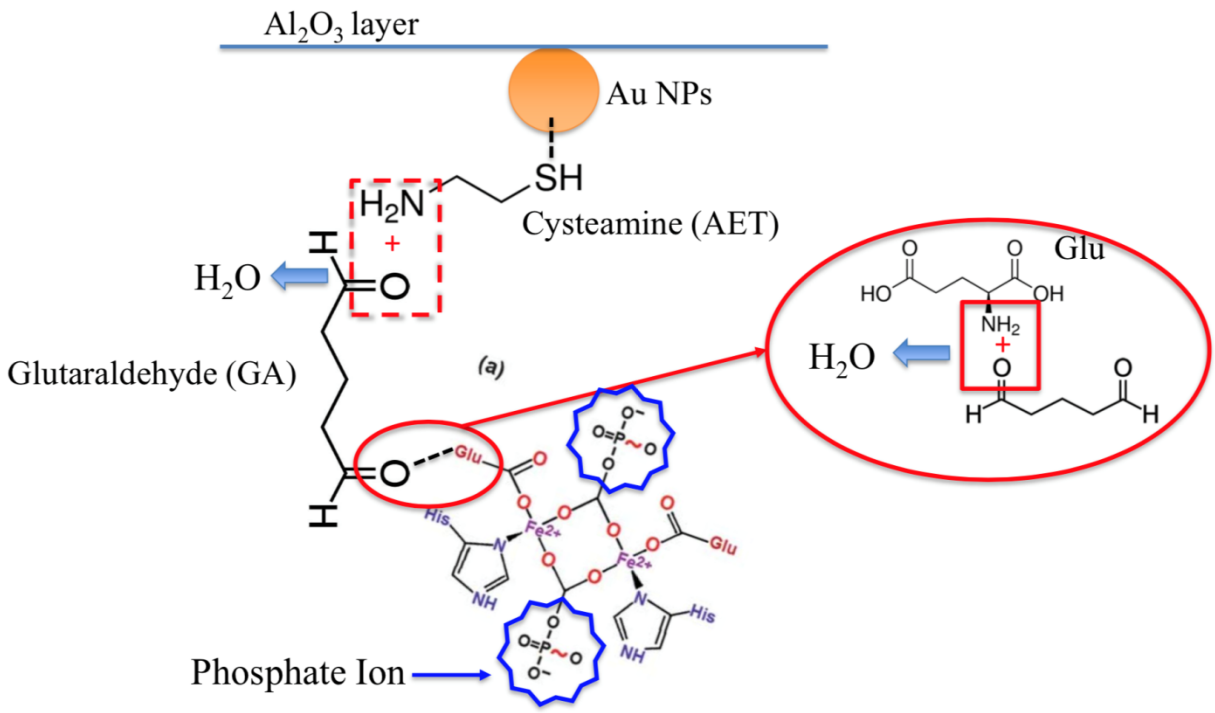

Figure 6. Modification layer on GO surface, from Al_2O_3 layer, AuNPs, AET to GA.

In this work, as introduced above, ALD is applied to screen the influence of water even though it is very small as shown in Figure 7a. Additionally, electrolyte conduction should also be considered, which would generate the background noise signal. From Figure 7b, it displayed that response from electrolyte conduction was nA level that can be ignored.

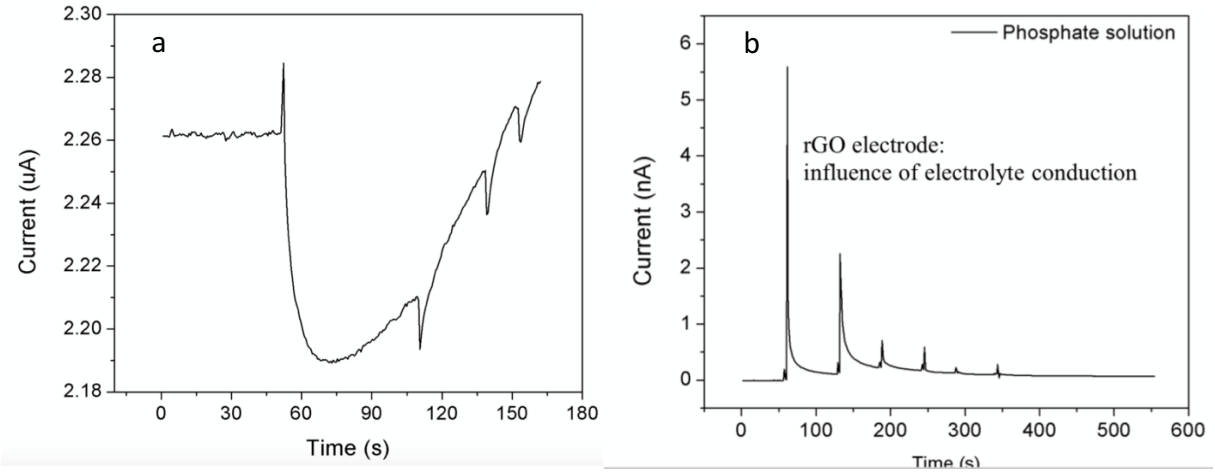

Figure 7. (a) Response from water as baseline; (b) Influence of electrolyte conduction.

2.1.3 Microstructure characterization of the electrode by SEM

As SEM image shown in Figure 8, one piece of rGO sheet was found to connect two interdigital fingers, one is source and the other is drain, respectively. The gap between these fingers is 3 μm, while the size of rGO is 5 μm to 10 μm after ultrasonic 40 mins in deionized water. The whole sensing area was independently locally bridged by tens of rGO sheets that determined the kilo ohm resistance (less than 100 KΩ).

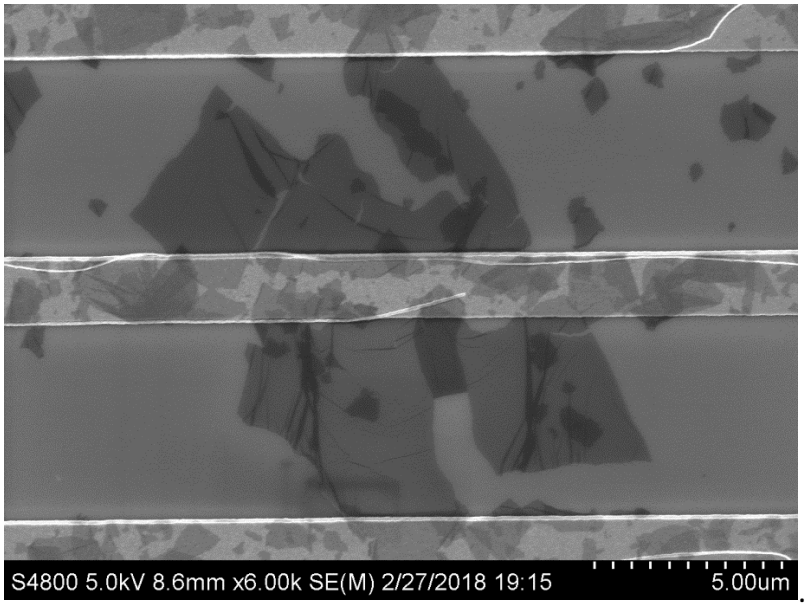

Figure 8. SEM image of gold electrodes and GO sheets between electrode gaps.

2.2 Characterization of GO by Raman spectroscopy

GO is basically insulating and highly disordered compared to the pristine graphene. But the availability of various oxygen-contained functional groups with both sp2 and sp3 carbon sites made them attractive towards synthesis of large scale production of graphene by suitable reduction kinetics. Depending on the preparation method, GO with chemical ranging from C8O2H3 to C8O4H, corresponding to a C/O ratio of 4:1-2:1. [39] After annealing, the C/O ratio can be improved

to 12:1. The fraction of sp2 and sp3 can be controlled by suitable reduction process and consequently, transition from insulator to semiconductor or to a metal. Raman spectroscopy is a classic experimental technique to investigate the bonding nature of carbon materials.

Table 3. Comparison of the reducing effect of GO by different methods [39].

Reduction method	**Form**	**C/O ratio**	**∂ (S/cm)**
Hydrazine hydrate	Powder	10.3	2
Hydrazine reduction in colloid state	Film	NA	72
Hydrazine vapor	Film	8.8	NG
Thermal annealing at 900 °C, UHV		14.1	NG
Thermal annealing at 1100 °C, UHV	TCF	NA	10^3
Thermal annealing at 1100 °C, Ar/H_2	TCF	NA	727

2.2.1 Raman results and analysis

As shown in Figure 9 of Raman analyses of rGO and comparison with GO, the latter displays a strong G peak at 1600.95 cm^{-1} due to the oxygenation of graphite. Additionally, a broadened D peak at 1349.67 cm^{-1} also appeared due to the creation of defects, vacancies and distortions of sp^2 domains after complete oxidation [40]. After reduction of graphene oxide, the G peak is shifted towards lower wave number compared to that position of GO. This shift was attributed to the recovery of hexagonal network of carbon atoms with defects. While the D peak intensity is increased in Rgo compared to GO suggesting that the reduction process modified the structure of GO with defects [24].

The D peak intensity was increased due to the reduction process modified the structure of GO with defects. Additionally, I(D)/I(G) ration was introduced to evaluate the average of the sp^2 cluster in the graphene material, where I(D) is the intensity of the D peak, and I(G) is the intensity of the G peak. The decrease in average size of sp^2 is due to the formation of sp^2 which are smaller in size compared to the ones present in GO before reduction [41].

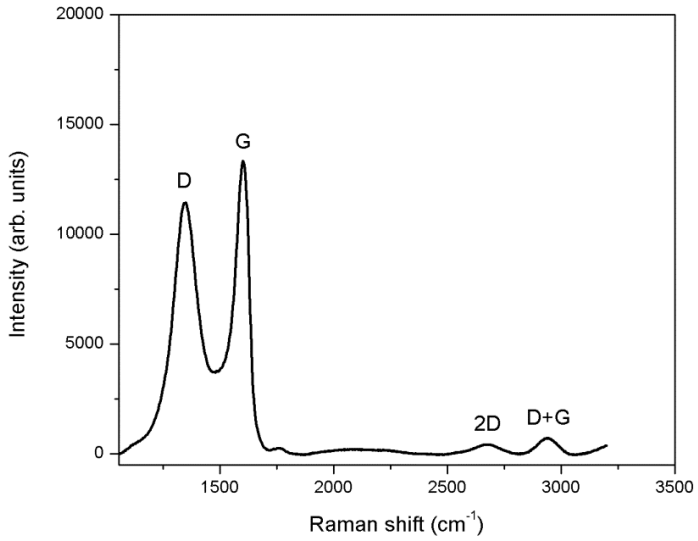

Figure 9. Raman spectrum of graphene oxide. D peak is at 1,349.67 cm^{-1}, G peak is at 1,600.95 cm^{-1}, and 2D peak is at 2,684.11 cm^{-1}.

2.3 Measurement procedure of the phosphate detection platform

As shown is Figure 10, this semiconductor characterization platform was used to test our sensors. It contains one back gate electrode and two contact electrodes. Before detecting phosphate ion solution, DI water or ultrapure water was added two more times to attain a stable baseline. Then, 2 ul of phosphate solutions with different concentrations was dropped at each time. The sensing signal was detected while reacting between ferritin and phosphate ions. Additionally, FET performance and IV property of rGO can also be tested by this platform. More test result details will be introduced in the following chapter.

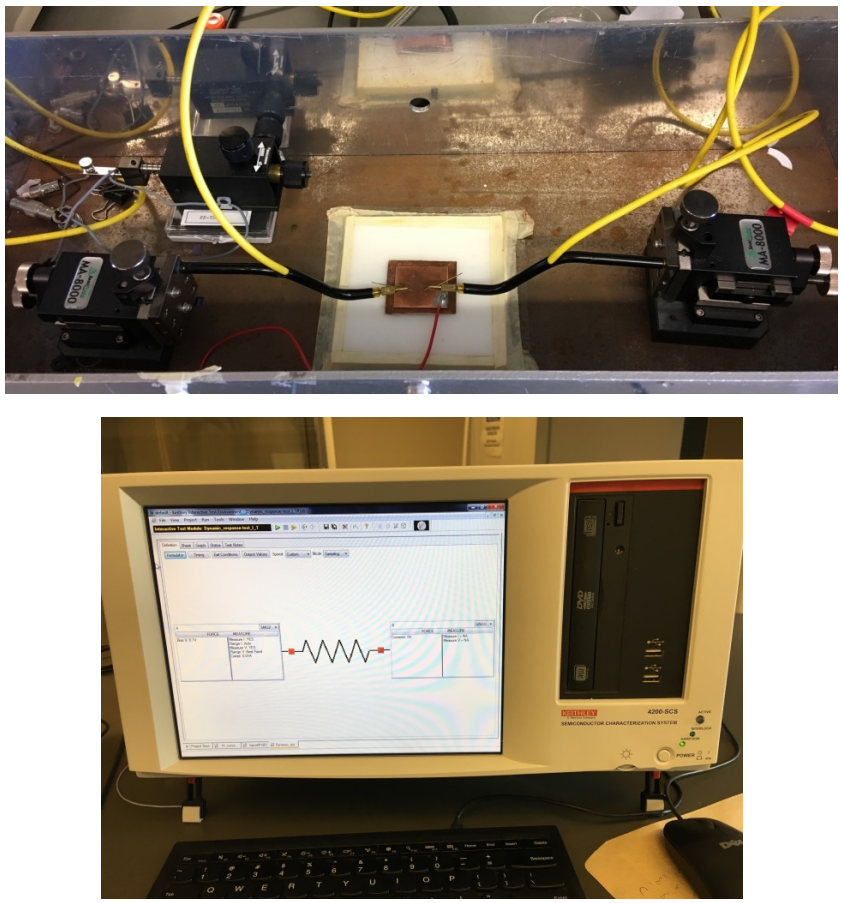

Figure 10. Characterization system for phosphate sensors.

From the published reports, [2, 5] there has two mechanisms to explain the response from GO-based FET sensor: charge transfer and gate effect. In our work, phosphate ions were negative charged which will increase the hole concentration in GO channel because of gate effect. However, once concentration increased to a high level, opposite response would be obtained due to the charge transfer between ferritin probes and phosphate ions, as shown in Figure 11.

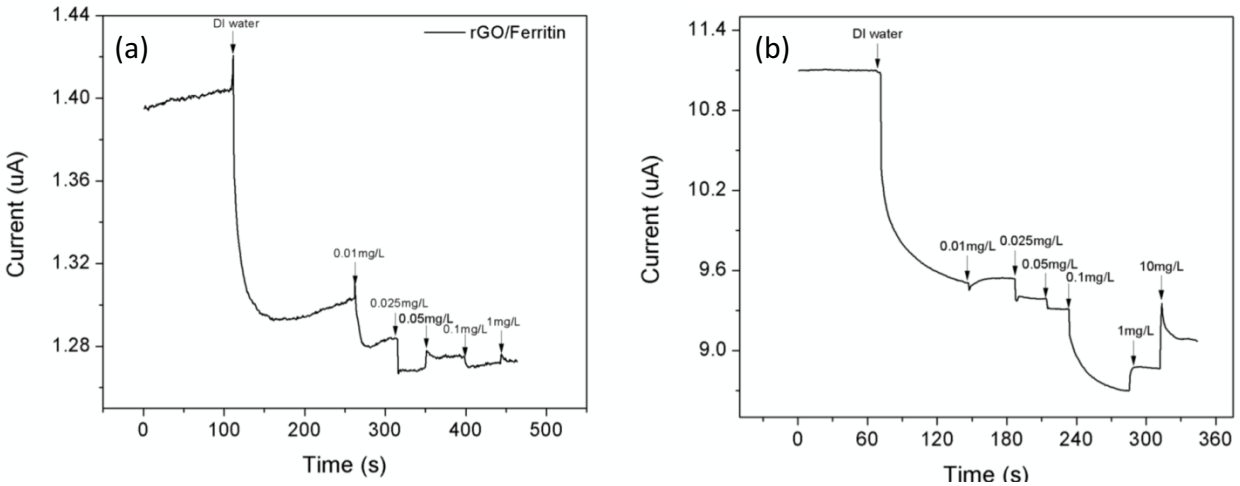

Figure 11. Opposite response of phosphate ions at different concentrations due to charge transfer and gate effect.

2.4 Summary and conclusion

In our work, interdigitated electrode was designed on the Si/SiO_2 substrate and GO sheets were applied as the working area to detect phosphate ions due to their unique electronic properties. The fabrication process is the same to the conventional semiconductor process including lithograph, developing and E-beam deposition. Although the total size of the sensing platform is 700mm*800mm, the size of sensor terminal is at micro level. Besides, from the Raman results, the GO sheet was single-layer which has similar properties to graphene.

CHAPTER 3 ELECTRICAL PROPERTIES OF GO-FET SENSING SYSTEM

3.1 Introduction

Here we report an ultrasensitive phosphate ions detection sensor based on graphene oxide-FET (GOFET). Aluminum oxide (Al_2O_3, ~4 nm thickness) was applied in our work to separate graphene oxide sheet (GO) from detection solution samples, and gold nanoparticle (AuNP ~2 nm diameter) was deposited on Al_2O_3 film surface for ferritin probes modification. As shown in Figure 12, ALD and AuNPs will increased the adsorption of phosphate ions [42-43]. After annealing under Argon environment, reduced graphene oxide demonstrated good current on/off ratio and p-type semiconductor FET performance. The results showed that ferritin probes had good affinity to phosphate ions in water solution. The limit of detection of our sensor system can achieve down to 0.025 mg/L for the real water test. This cost-less and micro-scale working electrode sensors can provide a new opportunity for the agriculture field and industry water emission real-time monitoring.

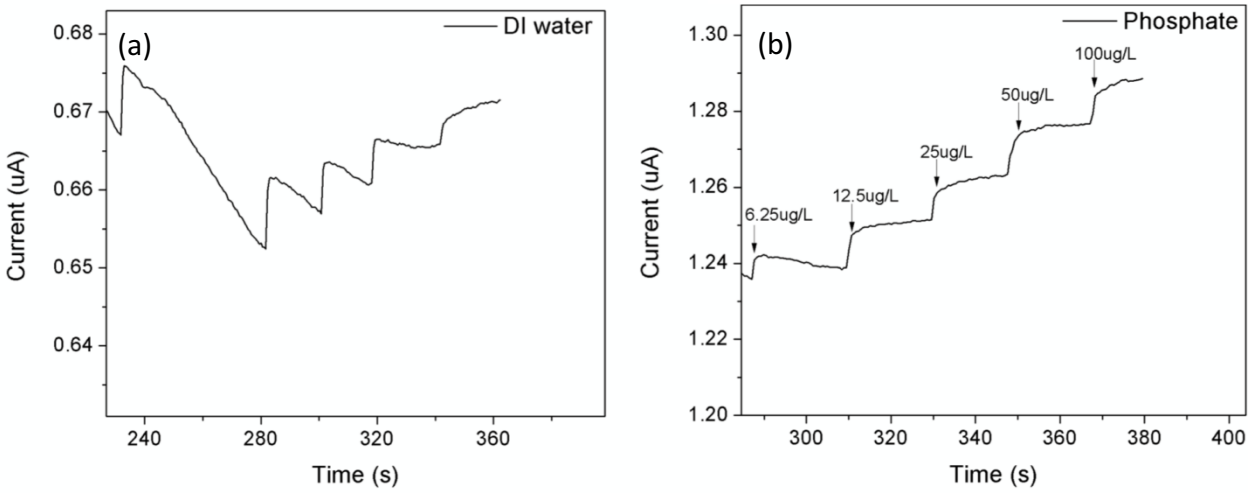

Figure 12. ALD and AuNPs improved the adsorption of phosphate ions and generated an increasing stable step signal.

3.2 Semiconductor properties of GO-FET

Graphene, a two-dimensional allotrope of carbon, plays an important role since it is the basis for the understanding of the electronic properties in other allotropes. Graphene is made out of carbon atoms arranged on a honeycomb structure made out of hexagons, and can be thought of as composed of benzene rings stripped put from their hydrogen atoms [44].

3.3 Charge neutral point

To further investigate the sensitivity of this sensor platform, in this work we researched the charge neutrality point transport of rGO in water samples, as shown in Figure 13. In contrast to ultra-clean or pristine graphene, the edges or defections randomly distribute on the graphene oxide surface are chemically reactive and can be relatively easily functionalized. Consequently, as the concentration changed of carriers, the charge neutrality point of Dirac point will strongly demonstrate p/n type shift. In addition, as the graphene are confined to an atomically thick plane, the electrical conductance, or also as known the carrier concentration, is extremely sensitive to its surroundings such as substrates, dielectric media, and adsorbed foreign molecules [31]. From which, the offset of Dirac point could reflect the concentration of phosphate ions in water solution. Although there exist many defects on the rGO even after annealing about 10 mins at 400 ºC under Argon ambiance, the introducing defects would not degrade the electronic property of rGO FETs.

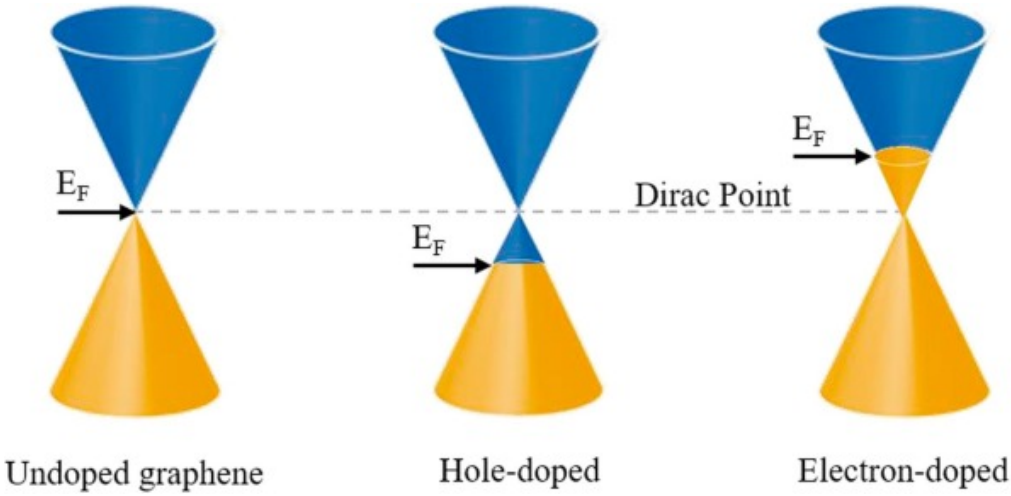

Figure 13. Diagram of the linear dispersion (Dirac cone) with conduction and valence bands touching at the K point (Dirac point) [45].

3.4 FET performance on different solutions

Figure 5 showed the schematic diagram of our phosphate sensor platform based on rGO-FET working principles. A bias voltage (~0.1 V) will be loaded between source/drain electrode. To investigate the FET performance of reduced graphene oxide, a back-gate voltage will scan from -40 V to 40 V, as in Figure 14a. Because of silicon substrate and SiO2 insulating layer, an equivalent gate voltage inducing electric field on rGO channel will be micro scale voltage. Although pure rGO presents a visible p-type semiconductor property, it will become ambipolar once dropping water solution on its surface, as shown in Figure 14b. The reason perhaps due to the adsorption of water molecules which would change the carriers' density of rGO. Furthermore, dropping phosphate ion solution from low to high concentration, the charge neutrality point (Dirac point) will left-shift to negative side since the increased gate voltage of FET. Also, current flow through rGO channel has an inverse correlation relationship with phosphate solution concentration.

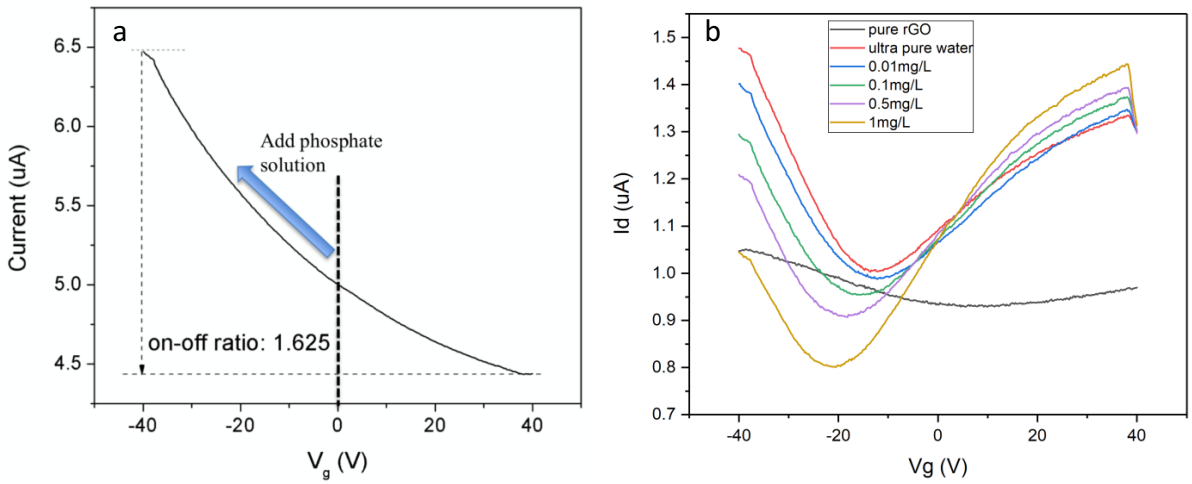

Figure 14. (a) rGO FET performance. (b) Dirac point is negatively shifted upon increasingphosphate solution concentration, and the current flow through the rGO channel has inverse correlation relationship to phosphate concentration.

3.5 Ohm characteristic

The volt-ampere characteristic of rGO sheet as shown in Figure 15 was I-V linear relationship, which demonstrated the contact between rGO and gold electrode was Ohmic contact. Additionally, with the purpose to obtain a high sensitivity, the resistance of sensor platform should be at least 1 KΩ. A high input impedance of sensor will minimize the interference with signal source and improve the signal-noise ratio (SNR). In our case, the size of rGO cross interdigital fingers was about 5 μm which would satisfy the high impedance requirement.

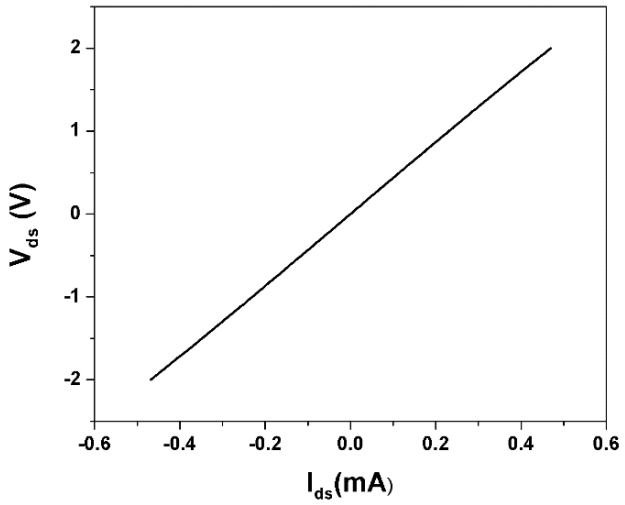

Figure 15. Ohm characterization of rGO without gate voltage. Usable resistance of rGO is kilo Ohm scale, which could be between 2 KΩ and 30 KΩ.

3.6 Summary and conclusion

As one of graphene family members, reduced graphene oxide demonstrates p-type semiconductor properties so that channel current will be decreased with the increasing gate voltage. In different solutions, charge neutral point of rGO is different upon the change of the carrier concentration. This sensing platform is very sensitive to phosphate ions, which can reach a lower limit of detection of 0.025 mg/L. Also, selectivity performance is good when test solution samples were introduced with interference ions.

CHAPTER 4 PHOSPHATE ION SENSOR PERFORMANCE

4.1 Introduction

Polymers offer a lot of advantages for sensor technologies: they are relatively low cost materials, their fabrication techniques are quite simple (there is no need for special clean-room and/or high temperature processes), they can be deposited on various types of substrates and the wide choice of their molecular structure and the possibility to build in side-chains, charged or neutral particles, and even grains of specific behavior into the bulk material or on its surface region, enables films to be produced with various physical and chemical properties including also sensing behavior [46].

Polydimethylsiloxane (PDMS) was integrated in our sensing platform for improving the performance of phosphate ions detection. The micro channel made by PDMS can be applied to control the flowing velocity of samples which can decrease the volume influence. Additional, PDMS reaction cell can define the sensing area size and can uniform the sensor resistance.

4.2 Phosphate sensing performance for selectivity and sensitivity study

This rGO-based FET device then was used to real-time detect phosphate ions in aqueous solution. A bias voltage was loaded between source and drain (~0.1 V) which supplied power for the alerted current or resistance of rGO. Theoretically, phosphate ion is negatively charged that as long as dropping phosphate ion-contained solution on the sensing area, the current through rGO channel will be increased due to the negative electric field of FET device was accumulated. However, as shown in Figure 4, time-dependent current measurement outcomes demonstrated a decrease tendency as pipetting phosphate solution from low concentrations to high concentrations. Based on Zeta potential testing, the potential of ferritin probe surface was found to be almost enhanced twice times after adsorbing phosphate ions, as shown in Table 1. The reason is likely

that structure and configuration of ferritin protein is deformed by phosphate ions, which will result chemical polarity altered on this protein surface. The phosphate ions in our lab solution with 7.4 pH value are existed in types of HPO_4^{2-} and $H_2PO_4^{-}$ [23]. Once zeta potential of ferritin was increased by phosphate ions, decreased current signal will be obtained due to the p-type electric field effect. Additionally, part of defects of rGO will be generated again by the first drop deionized water (DI water) that decreased the channel current. To eliminate the interference from DI water, dropped one more time DI water until all potential defect sites were occupied by DI water medium and the current signal to be stable, in Figure 16a. Then phosphate solution was added on sensing area from low concentration (25 μg/L) to high concentration (100 μg/L). A tiny final increased current signal is probably due to electrolyte conduction, in Figure 16b.

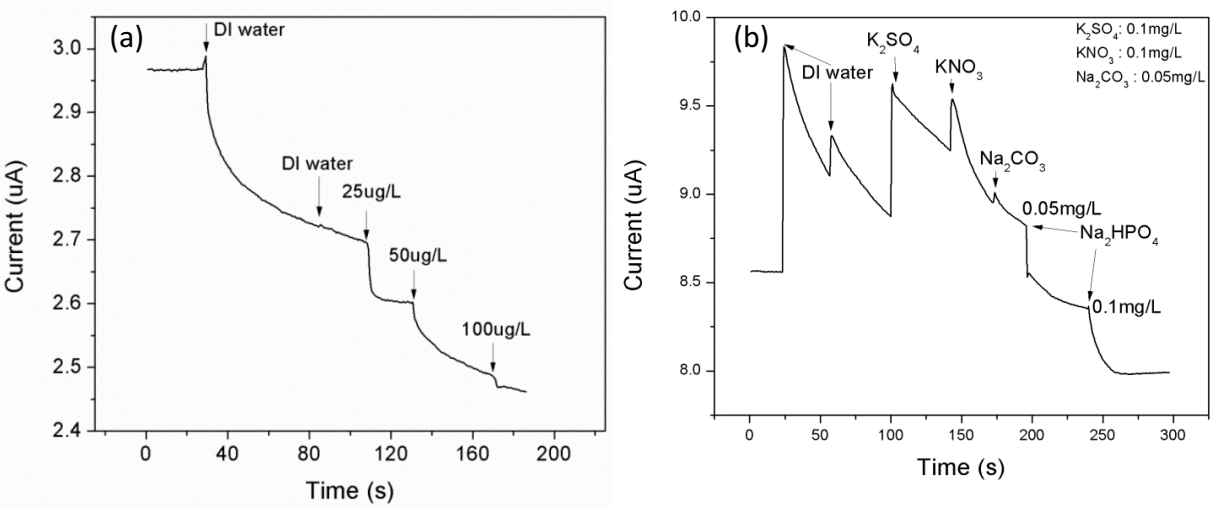

Figure 16. (a) Sensitivity, and (b) selectivity performance.

4.3 Real water samples detection

As above introduced, our sensor platform has an excellent limit of detection, with 0.001 mg/L, and response time can achieve second order-of magnitude. While, those tested phosphate solution was prepared in lab which was not introduced other interference ions. Then, this platform

was used to detect and real-time monitor the phosphate concentration in industry water emission well (Grande Cheese Co., 250 Camelot Drive, Fond du Lac, WI 54935). As shown in Figure 16a, DI water as baseline was dropped four times before adding real water samples with different concentration. DI water would give a current increment response while phosphate samples showed a decreasing current signal. At the end of the test, we dropped one more DI water and got the increased response from which could confirm phosphate ions will decrease current flowing through Rgo channel. The original concentration of the tested sample is 0.97 mg/L and was diluted to six different concentrations. To investigate the selectivity of this rGO-FET sensor, we studied other common interference anions such as NO_3^-, SO_4^{2-}, and CO_3^{2-} ions. Firstly, interference ions were added one by one and then mixed up these interference ions in real water sample. Finally, tested two different concentration real water samples (diluted five and ten times from original concentration with 0.97 mg/L), independently. As shown in Figure 17, compared with NO_3^-, SO_4^{2-}, and CO_3^{2-} ions which only have coulombic adsorption, the sensor to phosphate ion showed much greater response due to the highly specific binding affinity. The sensitivity of phosphate ion is several times higher than those of NO_3^-, SO_4^{2-}, and CO_3^{2-}, which indicated that our sensor platform could identify phosphate ions from other interference anions in water.

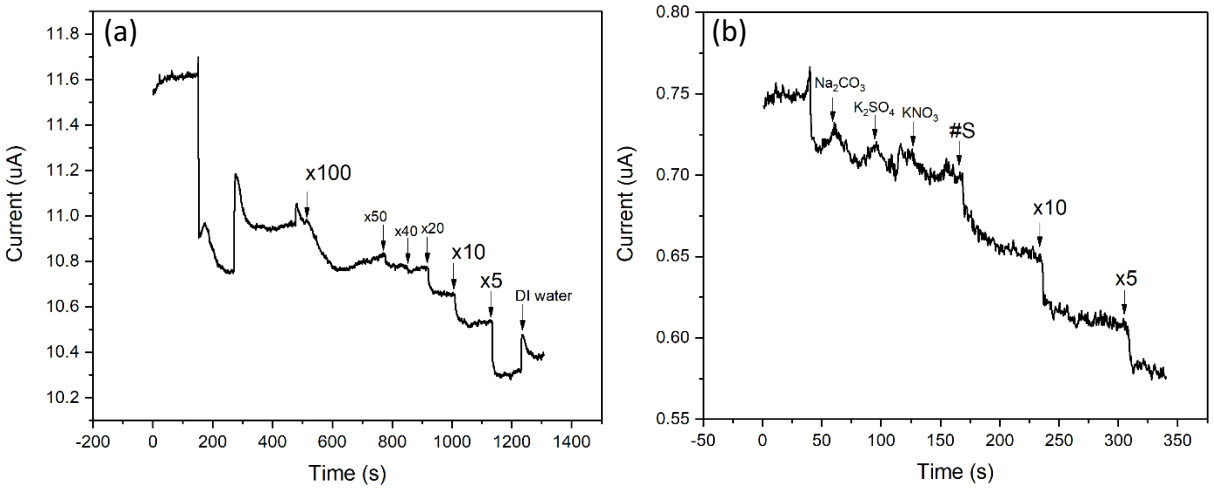

Figure 17. (a) Sensitivity and (b) selectivity performance to ream water samples.

4.4 Combined with PDMS micro channel

SU-8 photoresist was used for fabrication of PDMS patterns, as in Figure 18a. In our work, we designed one outlet, one inlet and one reaction cell. This PDMS micro channel will cover on sensing platform. As in Figure 18b, injecting sample solution into the inlet, then control the flowing speed by a pump. Since of this very tiny volume and low speed flowing, phosphate ions will be sufficiently adsorbed by the ferritin probes on AuNPs surface.

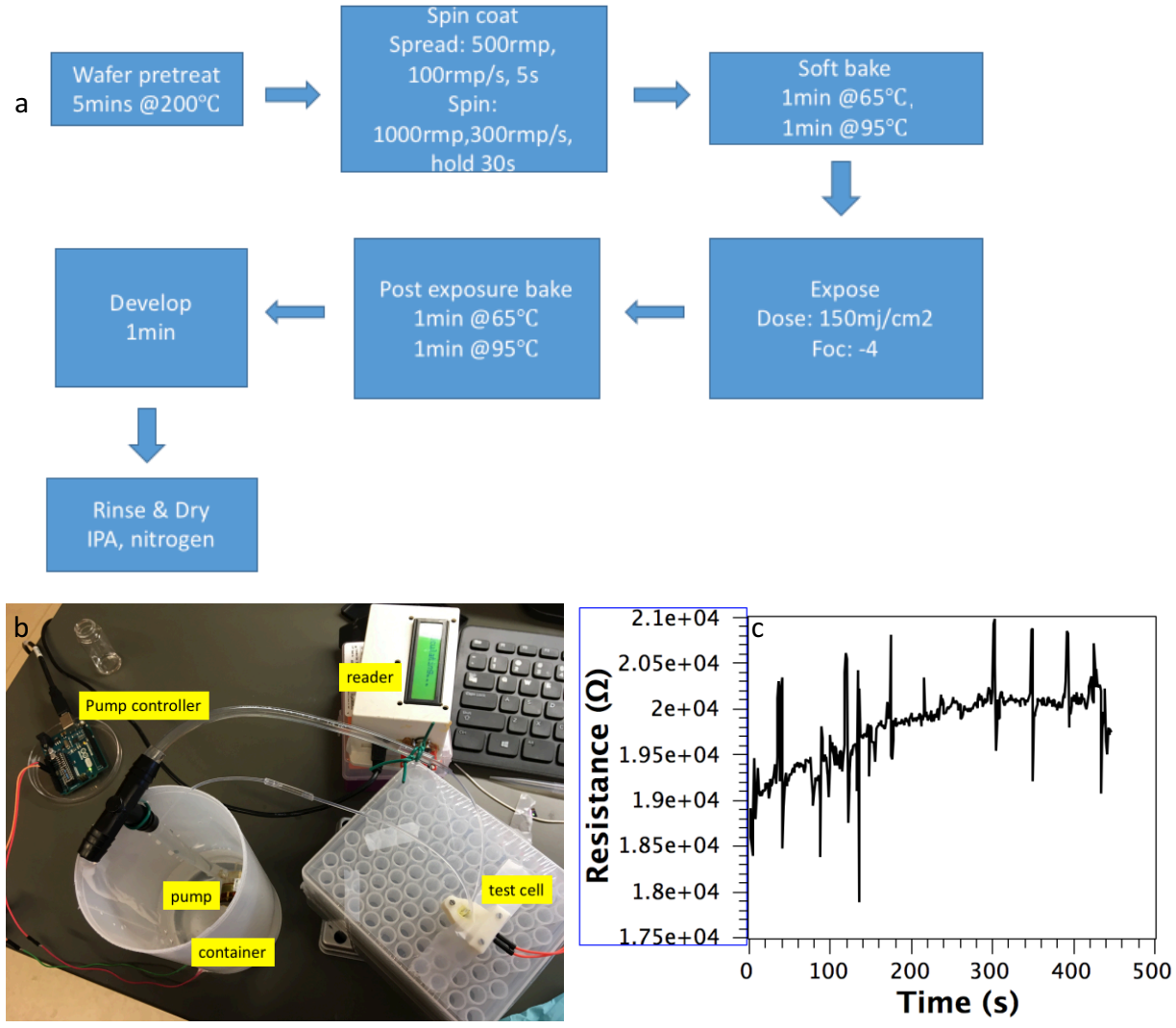

Figure 18. (a) Fabrication process of PDMS micro channel using SU-8 photoresist; (b) Test station including pump controller, pump, test cell and reader; (c) Test response.

4.5 Other strategies for enhancing sensing performance

4.5.1 Ionic strength

Ion exchange reaction has been frequently proposed as a mechanism for phosphate removal or adsorption on the adsorbents. The introduction of competing anions would reduce the uptake capacity of phosphate [47]. In this work, we introduced NaCl as the solution background. As shown in Figure 19, after adding the NaCl into the phosphate solution sample, sensitivity is higher than the pure phosphate samples. To eliminate the interference of NaCl, solution was dropped two times to get a stable baseline before testing different concentrations phosphate samples.

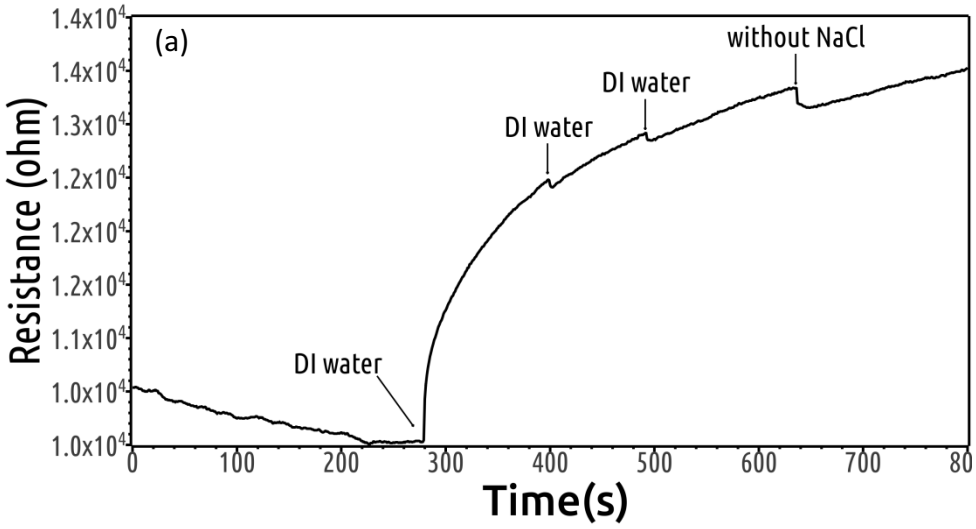

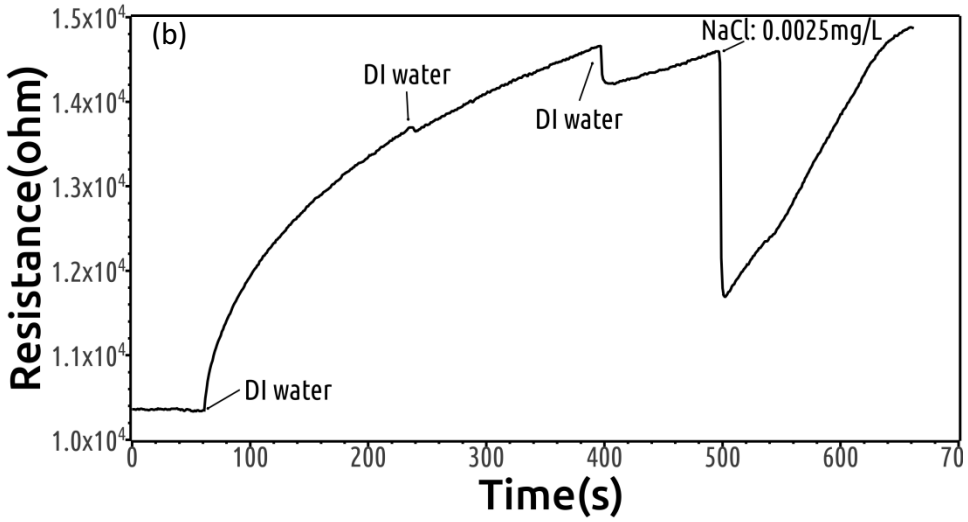

Figure 19. Ionic strength (NaCl) influence on sensing performance.

4.5.2 Back-gate voltage

Since phosphate ions are negatively charged, a positive back gate voltage can generate electric field to increase the adsorption of phosphate ions on the sensing area surface. In our work, we applied different voltages like 2 V, 0.067 V. As shown in Figure 20, 0.06 V is high enough to improve the sensitivity.

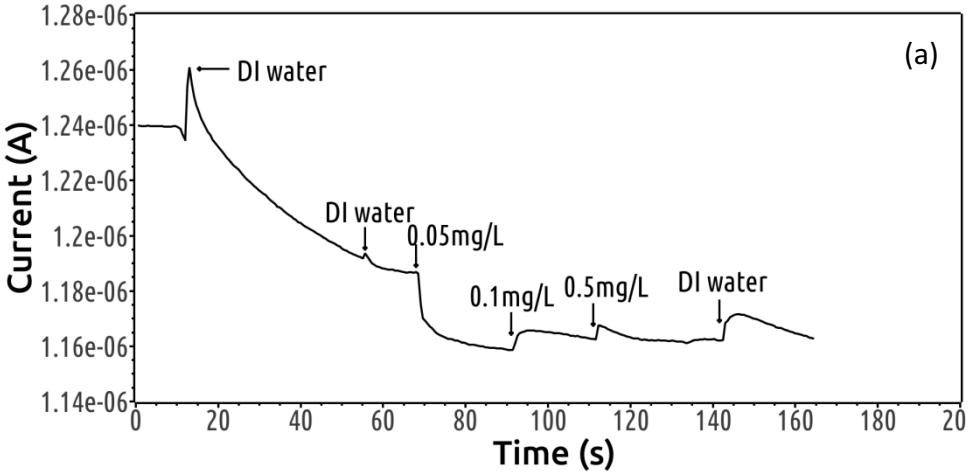

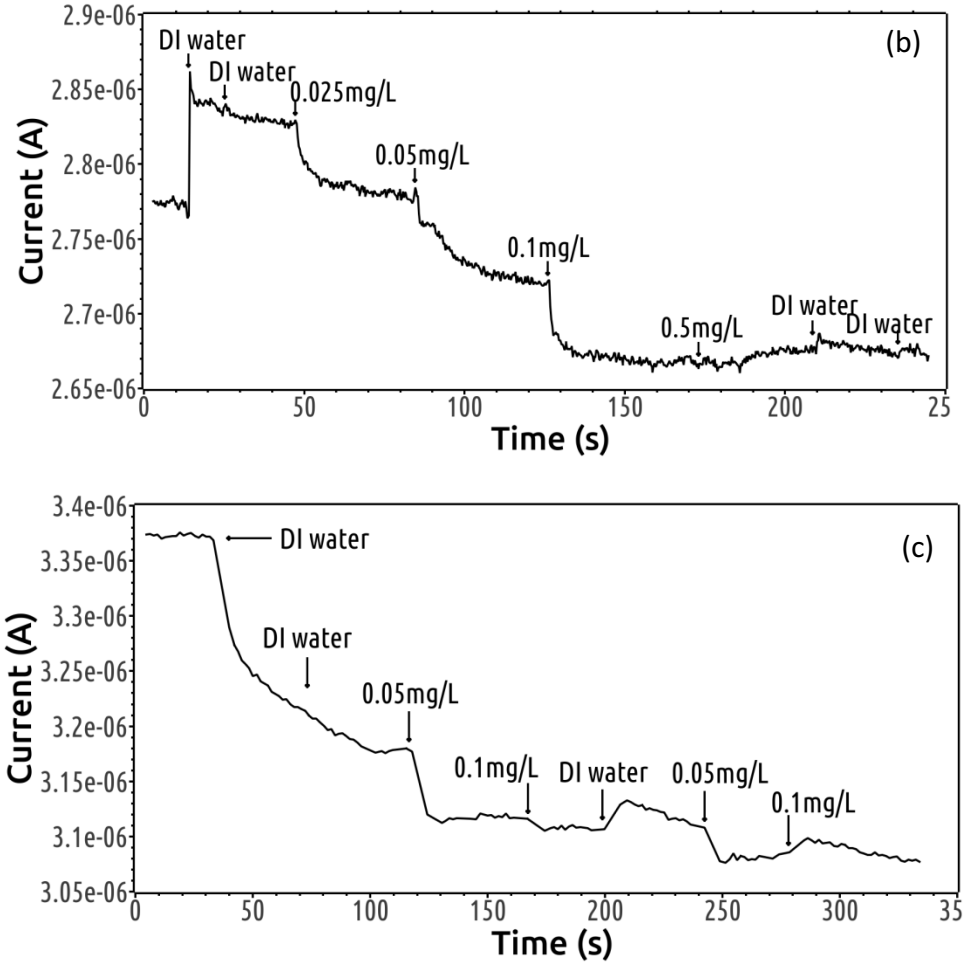

Figure 20. Effect of a back-gate-voltage on sensor performance, a) 0V, as reference. b) 0.06 V. c) 2 V.

CHAPTER 5 SUMMARY AND CONCLUSION

In summary, here we introduced an rGO-FET sensor for ultrasensitive real-time detection of phosphate ions with an LOD of 0.025 mg/L, for both lab-ready solutions and real solution samples from industry water discharge. It has a great implication for monitoring and controlling the concentration of phosphate ions in natural environment. This sensor platform can be a promising tool for low-concentration and real-time monitoring of phosphate ions and could be improved further by tuning the sensor structure.

From electrical characterization, rGO FET displayed a p-type semiconductor property. In our research, the response from our sensors could be due to charge transfer or field effect based on the concentration of phosphate samples. Additionally, the position of Daric point of rGO could also be as an index for quantifying the phosphate ions concentration. However, due to defects of electrodes and contact resistance, sensitivity performance is limited and degraded.

To optimize the sensitivity and selectivity, the device fabrication could be more precisely controlled and the density of rGO sheet across interdigitated fingers could also be controlled. Currently, microfluidic channel is widely applied to integrate with micro sensor chip for improving the reliability performance. To this end, a flow rate-controlled micro channel and cell molded by PDMS has been fabricated. The new sensor that combines nanomaterial-FET of unique properties with valid probes is promising for low-concentration monitoring of nutrients in water.

In the future, an intuitive calibration curve should be built for accurate determination of phosphate concentrations. Then a portable handheld-meter device could be set up to realize the purpose of real-time phosphate sensing platform. Finally, due to the degradation of ferritin probes on AuNPs surface after long-term use, the performance of the sensor will degrade (decrease in

sensitivity) over time. In addition, a method should be proposed to regenerate the ferritin probe for the reuse of the sensor.

REFERENCES

1. Cui, S.; Pu, H.; Wells, S. A.; Wen, Z.; Mao, S.; Chang, J.; Hersam, M. C.; Chen, J., Ultrahigh sensitivity and layer-dependent sensing performance of phosphorene-based gas sensors. *Nature communications* **2015,** *6*, 8632.
2. Chen, Y.; Ren, R.; Pu, H.; Guo, X.; Chang, J.; Zhou, G.; Mao, S.; Kron, M.; Chen, J., Field-Effect Transistor Biosensor for Rapid Detection of Ebola Antigen. *Scientific reports* **2017,** *7* (1), 10974.
3. Chang, J.; Huang, X.; Zhou, G.; Cui, S.; Hallac, P. B.; Jiang, J.; Hurley, P. T.; Chen, J., Multilayered Si Nanoparticle/Reduced Graphene Oxide Hybrid as a High‐Performance Lithium‐Ion Battery Anode. *Advanced materials* **2014,** *26* (5), 758-764.
4. Stankovich, S.; Dikin, D. A.; Piner, R. D.; Kohlhaas, K. A.; Kleinhammes, A.; Jia, Y.; Wu, Y.; Nguyen, S. T.; Ruoff, R. S., Synthesis of graphene-based nanosheets via chemical reduction of exfoliated graphite oxide. *carbon* **2007,** *45* (7), 1558-1565.
5. Zhou, G.; Chang, J.; Cui, S.; Pu, H.; Wen, Z.; Chen, J., Real-time, selective detection of Pb2+ in water using a reduced graphene oxide/gold nanoparticle field-effect transistor device. *ACS applied materials & interfaces* **2014,** *6* (21), 19235-19241.
6. Gómez-Navarro, C.; Weitz, R. T.; Bittner, A. M.; Scolari, M.; Mews, A.; Burghard, M.; Kern, K., Electronic transport properties of individual chemically reduced graphene oxide sheets. *Nano letters* **2007,** *7* (11), 3499-3503.
7. Ohno, Y.; Maehashi, K.; Yamashiro, Y.; Matsumoto, K., Electrolyte-gated graphene field-effect transistors for detecting pH and protein adsorption. *Nano letters* **2009,** *9* (9), 3318-3322.
8. Ohno, Y.; Maehashi, K.; Matsumoto, K., Label-free biosensors based on aptamer-modified graphene field-effect transistors. *Journal of the American Chemical Society* **2010,** *132* (51), 18012-18013.
9. Lin, C. T.; Loan, P. T. K.; Chen, T. Y.; Liu, K. K.; Chen, C. H.; Wei, K. H.; Li, L. J., Label‐Free Electrical Detection of DNA Hybridization on Graphene using Hall Effect Measurements: Revisiting the Sensing Mechanism. *Advanced Functional Materials* **2013,** *23* (18), 2301-2307.
10. Hess, L. H.; Jansen, M.; Maybeck, V.; Hauf, M. V.; Seifert, M.; Stutzmann, M.; Sharp, I. D.; Offenhäusser, A.; Garrido, J. A., Graphene transistor arrays for recording action potentials from electrogenic cells. *Advanced Materials* **2011,** *23* (43), 5045-5049.
11. Mao, S.; Pu, H.; Chang, J.; Sui, X.; Zhou, G.; Ren, R.; Chen, Y.; Chen, J., Ultrasensitive detection of orthophosphate ions with reduced graphene oxide/ferritin field-effect transistor sensors. *Environmental Science: Nano* **2017,** *4* (4), 856-863.
12. Fan, L.; Luo, C.; Li, X.; Lu, F.; Qiu, H.; Sun, M., Fabrication of novel magnetic chitosan grafted with graphene oxide to enhance adsorption properties for methyl blue. *Journal of hazardous materials* **2012,** *215*, 272-279.
13. Srinivas, G.; Burress, J.; Yildirim, T., Graphene oxide derived carbons (GODCs): synthesis and gas adsorption properties. *Energy & Environmental Science* **2012,** *5* (4), 6453-6459.
14. Sitko, R.; Turek, E.; Zawisza, B.; Malicka, E.; Talik, E.; Heimann, J.; Gagor, A.; Feist, B.; Wrzalik, R., Adsorption of divalent metal ions from aqueous solutions using graphene oxide. *Dalton Transactions* **2013,** *42* (16), 5682-5689.
15. Balandin, A. A., Low-frequency 1/f noise in graphene devices. *Nature nanotechnology* **2013,** *8* (8), 549.
16. Elias, D. C.; Nair, R. R.; Mohiuddin, T.; Morozov, S.; Blake, P.; Halsall, M.; Ferrari, A.; Boukhvalov, D.; Katsnelson, M.; Geim, A., Control of graphene's properties by reversible hydrogenation: evidence for graphane. *Science* **2009,** *323* (5914), 610-613.
17. Lu, Y.; Goldsmith, B. R.; Kybert, N. J.; Johnson, A. C., DNA-decorated graphene chemical sensors. *Applied Physics Letters* **2010,** *97* (8), 083107.

18. Fu, W.; Jiang, L.; van Geest, E. P.; Lima, L.; Schneider, G. F., Sensing at the Surface of Graphene Field‐Effect Transistors. *Advanced Materials* **2017,** *29* (6).
19. Cui, S.; Mao, S.; Wen, Z.; Chang, J.; Zhang, Y.; Chen, J., Controllable synthesis of silver nanoparticle-decorated reduced graphene oxide hybrids for ammonia detection. *Analyst* **2013,** *138* (10), 2877-2882.
20. Chen, K.; Lu, G.; Chang, J.; Mao, S.; Yu, K.; Cui, S.; Chen, J., Hg (II) ion detection using thermally reduced graphene oxide decorated with functionalized gold nanoparticles. *Analytical chemistry* **2012,** *84* (9), 4057-4062.
21. Chang, J.; Mao, S.; Zhang, Y.; Cui, S.; Zhou, G.; Wu, X.; Yang, C.-H.; Chen, J., Ultrasonic-assisted self-assembly of monolayer graphene oxide for rapid detection of Escherichia coli bacteria. *Nanoscale* **2013,** *5* (9), 3620-3626.
22. Block, G. A.; Hulbert-Shearon, T. E.; Levin, N. W.; Port, F. K., Association of serum phosphorus and calcium x phosphate product with mortality risk in chronic hemodialysis patients: a national study. *American Journal of Kidney Diseases* **1998,** *31* (4), 607-617.
23. Benjamin, M. M., *Water chemistry*. Waveland Press: 2014.
24. Moon, I. K.; Lee, J.; Ruoff, R. S.; Lee, H., Reduced graphene oxide by chemical graphitization. *Nature communications* **2010,** *1*, 73.
25. Huang, X.; Shi, K.; Yang, J.; Mao, G.; Chen, J., MnO 2-GO double-shelled sulfur (S@ MnO 2@ GO) as a cathode for Li-S batteries with improved rate capability and cyclic performance. *Journal of Power Sources* **2017,** *356*, 72-79.
26. Cao, Y.; Yang, H.; Zhao, Y.; Zhang, Y.; Ren, T.; Jin, B.; He, J.; Sun, J.-L., Fully Suspended Reduced Graphene Oxide Photodetector with Annealing Temperature-Dependent Broad Spectral Binary Photoresponses. *ACS Photonics* **2017,** *4* (11), 2797-2806.
27. Moriconi, L.; Niemeyer, D., Graphene conductivity near the charge neutral point. *Physical Review B* **2011,** *84* (19), 193401.
28. Wang, D.; Liu, X.; He, L.; Yin, Y.; Wu, D.; Shi, J., Manipulating graphene mobility and charge neutral point with ligand-bound nanoparticles as charge reservoir. *Nano letters* **2010,** *10* (12), 4989-4993.
29. Shallcross, S.; Sharma, S.; Weber, H. B., Anomalous Dirac point transport due to extended defects in bilayer graphene. *Nature communications* **2017,** *8* (1), 342.
30. Huang, H.; Tao, L.; Liu, F.; Ji, L.; Hu, Y.; Cheng, M. M.-C.; Chen, P.-Y.; Akinwande, D., Chemical-sensitive graphene modulator with a memory effect for internet-of-things applications. *Microsystems & Nanoengineering* **2016,** *2*, 16018.
31. Tan, X., Chuang, H., Lin, M., Zhou, Z., & Cheng, M., Edge Effects on the pH Response of Graphene Nanoribbon Field Effect Transistors. *The Journal of Physical Chemistry* **2013,** *117* (51).
32. Zhu, Y.; Murali, S.; Cai, W.; Li, X.; Suk, J. W.; Potts, J. R.; Ruoff, R. S., Graphene and graphene oxide: synthesis, properties, and applications. *Advanced materials* **2010,** *22* (35), 3906-3924.
33. Chen, B. B.; Li, R. S.; Liu, M. L.; Zou, H. Y.; Liu, H.; Huang, C. Z., Highly selective detection of phosphate ion based on a single-layered graphene quantum dots-Al3+ strategy. *Talanta* **2018,** *178*, 172-177.
34. Jia, X.; Chen, D.; Bin, L.; Lu, H.; Zhang, R.; Zheng, Y., Highly selective and sensitive phosphate anion sensors based on AlGaN/GaN high electron mobility transistors functionalized by ion imprinted polymer. *Scientific reports* **2016,** *6*, 27728.
35. Barhoumi, L.; Baraket, A.; Nooredeen, N. M.; Ali, M. B.; Abbas, M. N.; Bausells, J.; Errachid, A., Silicon Nitride Capacitive Chemical Sensor for Phosphate Ion Detection Based on Copper Phthalocyanine–Acrylate‐polymer. *Electroanalysis* **2017,** *29* (6), 1586-1595.
36. Ahmad, A.; Hanifah, S. A.; Hasbullah, S. A.; Suhud, K.; Zaini, N. M.; Heng, L. Y. In *Phosphate sensor based on immobilized aluminium-morin in poly (glycidyl methacrylate) microspheres*, AIP Conference Proceedings, AIP: 2014; pp 486-491.

37. Fu, W.; Jiang, L.; van Geest, E. P.; Lima, L.; Schneider, G. F., Sensing at the Surface of Graphene Field-Effect Transistors. *Advanced Materials* **2016**.
38. Stern, E.; Wagner, R.; Sigworth, F. J.; Breaker, R.; Fahmy, T. M.; Reed, M. A., Importance of the Debye screening length on nanowire field effect transistor sensors. *Nano letters* **2007,** *7* (11), 3405-3409.
39. Pei, S.; Cheng, H.-M., The reduction of graphene oxide. *Carbon* **2012,** *50* (9), 3210-3228.
40. Krishnamoorthy, K.; Veerapandian, M.; Mohan, R.; Kim, S.-J., Investigation of Raman and photoluminescence studies of reduced graphene oxide sheets. *Applied Physics A* **2012,** *106* (3), 501-506.
41. Zhu, C.; Guo, S.; Fang, Y.; Dong, S., Reducing sugar: new functional molecules for the green synthesis of graphene nanosheets. *ACS nano* **2010,** *4* (4), 2429-2437.
42. Bellino, M. G.; Calvo, E. J.; Gordillo, G., Adsorption kinetics of charged thiols on gold nanoparticles. *Physical Chemistry Chemical Physics* **2004,** *6* (2), 424-428.
43. Gagner, J. E.; Lopez, M. D.; Dordick, J. S.; Siegel, R. W., Effect of gold nanoparticle morphology on adsorbed protein structure and function. *Biomaterials* **2011,** *32* (29), 7241-7252.
44. Neto, A. C.; Guinea, F.; Peres, N. M.; Novoselov, K. S.; Geim, A. K., The electronic properties of graphene. *Reviews of modern physics* **2009,** *81* (1), 109.
45. Giubileo, F.; Di Bartolomeo, A., The role of contact resistance in graphene field-effect devices. *Progress in Surface Science* **2017,** *92* (3), 143-175.
46. Harsányi, G., Polymer films in sensor applications: a review of present uses and future possibilities. *Sensor Review* **2000,** *20* (2), 98-105.
47. Tian, S.; Jiang, P.; Ning, P.; Su, Y., Enhanced adsorption removal of phosphate from water by mixed lanthanum/aluminum pillared montmorillonite. *Chemical Engineering Journal* **2009,** *151* (1-3), 141-148.